Robust Tin-Based Perovskite Solar Cells with Hybrid Organic Cations to Attain Efficiency Approaching 10%

Efat Jokar, Cheng-Hsun Chien, Cheng-Min Tsai, Amir Fathi, and Eric Wei-Guang Diau*

The stability of a tin-based perovskite solar cell is a major challenge. Here, hybrid tin-based perovskite solar cells in a new series that incorporate a nonpolar organic cation, guanidinium (GA⁺), in varied proportions into the formamidinium (FA⁺) tin triiodide perovskite (FASnI₃) crystal structure in the presence of 1% ethylenediammonium diiodide (EDAI₂) as an additive, are reported. The device performance is optimized at a precursor ratio (GAI:FAI) of 20:80 to attain a power conversion efficiency (PCE) of 8.5% when prepared freshly; the efficiencies continuously increase to attain a record PCE of 9.6% after storage in a glove-box environment for 2000 h. The hybrid perovskite works stably under continuous 1 sun illumination for 1 h and storage in air for 6 days without encapsulation. Such a tin-based perovskite passes all harsh standard tests, and the efficiency of a fresh device, 8.3%, is certified. The great performance and stability of the device reported herein attains a new milestone for lead-free perovskite solar cells on a path toward commercial development.

Lead-based perovskite solar cells (PSC) have progressed rapidly in recent years to attain a power conversion efficiency (PCE) over 23% and have inspired hopes of scientists and engineers to develop cost-effective next-generation solar cells.[1,2] Two issues remain to be addressed before PSC can be commercialized—their stability and the toxicity of lead in PSC. Several effective approaches[3,4] have been employed to improve the stability of lead-based PSC devices, but toxic element lead must be replaced with a nontoxic material such as tin.[5–8] Tin-based perovskites have the advantages of smaller optical bandgaps[7] and greater charge mobility than their lead-based perovskites,[8] but tin-based PSC are apt to suffer oxidation from Sn^{2+} to Sn^{4+}. Sn^{4+} acts as a p-dopant within the perovskite in a process so called *self-doping* and increases the concentrations of holes that could lead to severe recombination of charge carriers in these solar cells.[9] Early tests of methylammonium tin triiodide

(MASnI₃) PSC yielded device performance with PCE 5–6%,[9,10] but the devices were unstable and lacked reproducibility due to oxidation of Sn^{2+}. To suppress that oxidation, much effort has been exerted to improve the enduring stability of the performance of tin-based PSC,[11–16] for example, through changing the electronic structure of perovskite, providing a uniform and close-packed film, introducing hydrogen bonding and a hydrophobic shell, and so forth.[12–14,17,18]

Formamidinium (FA⁺) is larger than MA⁺. FASnI₃ has a greater energy of formation of Sn vacancies because of weaker coupling between Sn and I;[19] FASnI₃ has thereby a smaller p-type conductivity than MASnI₃ and acts as a semiconductor. Wang et al.[18] studied the interaction of both FASnI₃ and MASnI₃ perovskites with water and concluded that these two cations affect the electronic structure of the oxygen-bonded perovskite lattice; FASnI₃ has a smaller rate of oxidation of Sn^{2+} than MASnI₃. They also suggested that stable Sn-based perovskite devices might be realized through an appropriate choice of organic cation to ensure effective protection against water penetration.[18] As a result, organic cation FA⁺ has been used to make a FASnI₃ or hybrid FA⁺/MA⁺ device with PCE 4–8%.[20] Moreover, applying large hydrophobic ammonium cations such as butylammonium (BA⁺) or phenylethylammonium (PEA⁺) within FASnI₃ to develop a quasi-2D[21] or hybrid 2D/3D[12,13,15] PSC was reported to make stable devices with PCE as great as 9.0%.[12]

Beyond MA⁺ and FA⁺, organic cation guanidinium ($CH_6N_3^+$, GA), of size ≈278 pm[22] that is slightly larger than that of FA⁺ (≈253 pm)[22] but has zero electric-dipolar moment, might be a suitable candidate for a tin-based PSC.[23,24] The empirical Goldschmidt tolerance factor of GASnI₃ is 1.051; GASnI₃ has a hexagonal geometry with crystal structures of two types, both with large bandgaps: 1.9 eV for the 3D hexagonal structure, space group $P6_3/m$, and 2.1 eV for the 2D monoclinic structure, space group $P2_1/n$, near 296 K.[25]

We applied organic cation precursor GAI mixed with FAI in varied proportions with equimolar SnI₂ precursor in the presence of SnF₂ and ethylenediammonium diiodide (EDAI₂) as additives to enhance both the photovoltaic performance and the enduring stability of a tin-based perovskite. As demonstrated at the top of **Figure 1**, we prepared the tin perovskites according to stoichiometric ratios of their precursors; these prepared perovskites conform to a general expression,

Dr. E. Jokar, C.-H. Chien, C.-M. Tsai, A. Fathi, Prof. E. W.-G. Diau
Department of Applied Chemistry and Institute of Molecular Science
National Chiao Tung University
1001 Ta-Hsueh Rd., Hsinchu 30010, Taiwan
E-mail: diau@mail.nctu.edu.tw
Prof. E. W.-G. Diau
Center for Emergent Functional Matter Science
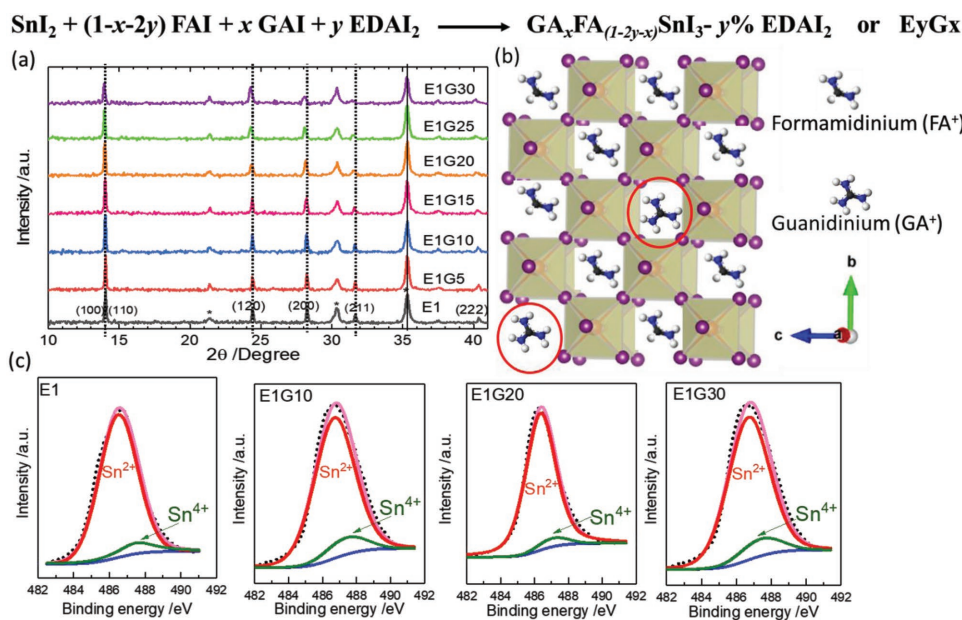National Chiao Tung University
1001 Ta-Hsueh Rd., Hsinchu 30010, Taiwan

Figure 1. a) X-ray diffraction patterns of E1Gx samples with x = 0 to 30; b) 2 × 2 × 2 supercell of E1G20 perovskite; c) high-resolution X-ray photoelectron spectra (Sn 3d) of the surface of E1Gx films with x = 0, 10, 20, and 30. The symbol * in (a) indicates the diffraction symbol of the ITO substrate.

$GA_xFA_{1-x-2y}SnI_3-yEDAI_2$, abbreviated as EyGx with integers x and y representing the corresponding proportions without showing percentage symbol (%). Upon increasing the ratios GAI:FAI, the size of the perovskite crystal increases continuously, but no phase transition was observed (Figure 1a). The device performance became optimal at GAI 20% and EDAI$_2$ 1% (E1G20), for which a fresh cell showed the best PCE 8.5% and certified efficiency 8.3%. The device performance was certified under a strict condition to prove the superior stability of our devices. Moreover, when the device was stored in a glove box, the performance increased continuously, to attain PCE 9.6% after storage period ≈2000 h; the great performance and stability of the device have attained a new milestone for lead-free perovskite solar cells on a path toward commercialization.

Our preceding work[26] indicated that adding EDAI$_2$ 1% in a trace proportion would assist the growth of uniform and dense perovskite films free of pinholes; FASnI$_3$–1%EDAI$_2$ (E1) PSC was hence chosen as a standard cell for comparison with other devices made of mixed GAI/FAI in varied ratios. The scanning electron microscopy (SEM) top-view images of both Gx and E1Gx (x = 0–30) films appear in Figure S1 (Supporting Information). Gx films evidently have a pinhole problem, which has been solved on adding EDAI$_2$ 1% (E1Gx) to control the morphology of the perovskite films. The problem of pinholes of the G20 films cannot be fixed in the absence of EDAI$_2$ due to the unbalanced rates between nucleation and crystal growth,[27] i.e., when the crystal growth rate was too rapid and the nucleation was not complete yet, then rapid growth of the crystal would generate pinholes on the G20 films. In contrast, the existence of a small amount of EDAI$_2$ in the EyG20 films could slow down the crystal growth so that the uniform nucleation can be achieved to form dense-packed and pinhole-free perovskite films. This phenomenon is the same as what we observed for the E1 films in comparison with the pristine FASnI$_3$ films,[26] and we may conclude that EDAI$_2$ can control the growth rate of perovskite for the case of EyG20 as well.

The Goldschmidt tolerance factors (t)[28,29] listed in Table S1 (Supporting Information) indicate that the formation of mixed-cation GA$^+$/FA$^+$ tin triiodide perovskites is feasible. Large-scale single crystals for three compositions (E1Gx, x = 10, 20, and 30) were grown in γ-butyrolactone (GBL) for a period of 45–60 days, according to photographs shown in Figure S2 (Supporting Information); Table S2 (Supporting Information) lists the lattice parameters of these single crystals. Single-crystalline and thin-film samples of our mixed-cation tin perovskite appear black and have great stability in air. Kubicki et al.[29] found that black hybrid FA$^+$/GA$^+$ lead triiodide perovskite crystals were thermodynamically unstable and became yellow in a few hours; moreover, crystal reorientation was observed in their mother structure (FAPbI$_3$).[30,31] Phase transition occurred at room temperature has been reported for FAPbI$_3$ but not for FASnI$_3$ because it happened at much lower temperatures (125–150 K)[32] for which the black phase of FASnI$_3$ is stable at room temperature.[33] Based on our single-crystal results, the GA$_x$FA$_{1-x}$SnI$_3$ perovskites adopt the same structure as FASnI$_3$ until adding 30% of GA$^+$. We therefore expect that they have the same phase stability as their parent perovskite FASnI$_3$.

X-ray diffraction (XRD) data for a single crystal confirm that GA$^+$ cations inserted into a 3D perovskite lattice structure according to the E1G20 supercell shown in Figure 1b. The GA$_x$FA$_{1-x}$SnI$_3$ perovskites adopt the same structure as FASnI$_3$ with an orthorhombic unit cell, space group Amm2.[34] On introducing GA$^+$ into the FASnI$_3$ structure, because GA$^+$ cation is larger than FA$^+$, the unit cell expands and the lattice parameters gradually increase. This feature of the crystal structure has been observed in a hybrid MA$^+$/GA$^+$ lead-based perovskite MA$_{1-x}$GA$_x$PbI$_3$.[35] Powder XRD spectra of Gx thin-film samples confirm this change in crystal lattice, for which the diffraction signals shifted systematically to small angles upon increasing the proportions of GAI (Figure S3, Supporting Information) until a large proportion of GAI (G30); no other

phase or precursor signal was observed. Figure 1a shows that the same behavior was observed for the thin-film samples with additive $EDAI_2$ 1% (E1Gx). The presence of $EDAI_2$ can alter the preferred orientation of crystal growth along the direction of plane (100)/(110). In contrast, in the absence of $EDAI_2$, the growth of the crystal along the direction of plane (120) was preferred (Figure S3, Supporting Information). As mentioned elsewhere,[26] $EDAI_2$ additive plays a key role to control the kinetics of film formation and produce the crystal grain size more uniform than the pristine $FASnI_3$ and therefore affects the crystal orientation of perovskite on the film.[36,37] The XRD patterns of the E1Gx films with varied GAI proportions ($x = 0–30$) were simulated (TOPAS software) to calculate the lattice parameters of the perovskite crystals at varied GAI proportions (Figure S4, Supporting Information); the simulated lattice parameters are listed in Table S3 (Supporting Information). The crystal lattices of the thin-film samples show the same feature as the single-crystal data with lattice parameters gradually increasing on increasing the proportion of GAI.

X-ray photoelectron spectra (XPS) of E1Gx samples (as shown in Figure 1c) were deconvoluted into two components corresponding to Sn^{2+} (red trace) and Sn^{4+} species (green trace). The calculated fractions of those Sn^{2+} and Sn^{4+} species are shown in Table S4 (Supporting Information). These data indicate that the presence of $EDAI_2$ in a trace proportion stabilizes the tin perovskite against oxidation of Sn^{2+} on the surface, as reported elsewhere.[26] The E1G20 sample exhibited the largest Sn^{2+}/Sn^{4+} ratio, outperforming the other samples.

Figure 2a shows the variation of the absorption spectra of the E1Gx samples for $x = 0–30$. The absorption band edges shifted systematically toward small wavelength when the proportion of GAI increased; the bandgap energies were determined to be 1.44, 1.45, 1.47, 1.50, and 1.53 eV for $x = 0, 5, 10, 20,$ and 30, respectively. The corresponding PL spectra shown in Figure 2b also display a systematic blueshift feature upon increasing proportions of GAI, like the absorption spectra. The evidence of these systematic blueshift spectral features shown in both absorption and PL spectra indicates that GA^+ became involved in the perovskite crystal structure, consistent with the XRD results shown in Figure 1a. Figure 2c shows transient PL decays obtained from measurements of TCSPC. The PL lifetimes were similar for all samples, varying in a range 0.7–1.4 ns (Table S5, Supporting Information). The E1 sample has lifetime 0.7 ns; when the GAI was introduced, the PL lifetimes began to increase to 1.4 ns for the E1G15 sample, and then decreased to 0.7 ns for the E1G30 sample. These observed changes in the PL lifetime might indicate that fewer defect states were produced at particular proportions of GAI (10–25%).

The effect of GAI on the electronic structure of perovskites can be tested with ultraviolet photoelectron spectra (UPS). Figure 2d shows the energy levels of the valence band (VB) of the E1Gx samples obtained on analysis of the UPS data (Figure S5, Supporting Information); the energy levels of the conduction band (CB) were derived on scaling the VB levels with the corresponding bandgap energies. In the literature there is inconsistency about the energy levels of tin perovskites due to facile oxidation of Sn^{2+}.[20,33,38] Zhao et al.[20] mentioned that severe oxidation of Sn^{2+} altered the VB from −4.88 to −6.0 eV. Based on our XPS results shown in Figure 1c, the tendency to oxidation of Sn^{2+} in our samples is small; the obtained VB for the E1 sample is consistent with that reported elsewhere.[19,20] As Figure 2d shows, the presence of GAI 10–20% in the perovskite crystal can alter the electronic structure of perovskite and shift the VB level to match the energy level of the hole-transport layer (PEDOT:PSS).
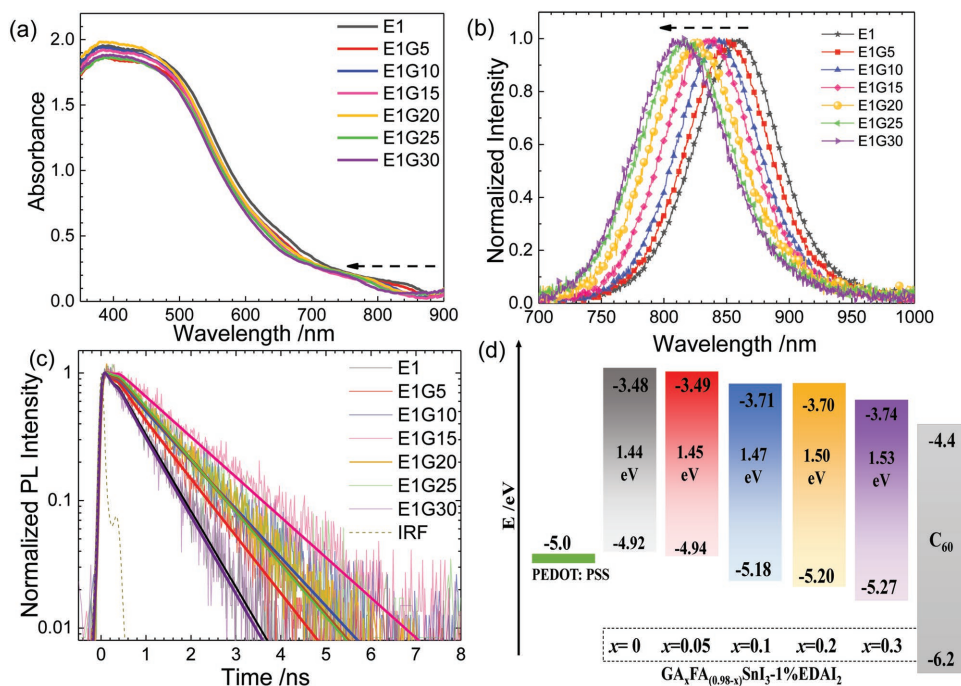

Figure 2. a) Absorption spectra, b) steady-state photoluminescence (PL) spectra, c) time-resolved PL decay profiles, and d) potential-energy diagrams (energies in eV with respect to vacuum) of $GA_xFA_{(0.98-x)}SnI_3$–1% $EDAI_2$ (E1Gx) films with GAI in varied proportions ($x = 0–0.3$) as indicated.

**ADVANCED
SCIENCE NEWS**

www.advancedsciencenews.com

**ADVANCED
MATERIALS**

www.advmat.de

In the Pb halide perovskite system, the s–p antibonding coupling contributes significantly to their energy-level properties. Accordingly, for the Sn-based system, we may assume that the energy levels of VB are determined from the interaction of I 5p and Sn 5s orbitals. For example, the average Sn−I bond length in $FASnI_3$ is longer than that in $MASnI_3$, which might result in stronger antibonding coupling, leading to an increase of the VB of $MASnI_3$ to a higher energy level in comparison with that in $FASnI_3$.[19] For a mixed cationic perovskite system (MA^+ and FA^+), it was shown that the VB levels decrease upon increasing the amount of FA^+ inside the perovskite.[20] Based on these two papers, we may conclude that the downward shifts of the VBM levels upon increasing the amount of GA^+ in our hybrid FA/GA tin perovskite system are reasonable.

To demonstrate E1Gx perovskites as a light absorber for photovoltaic applications, we fabricated inverted planar heterojunction (PHJ) perovskite solar cells based on the device configuration ITO/PEDOT:PSS/E1Gx (120–150 nm)/C_{60} (20 nm)/BCP/Ag. The device structure and the cross-sectional SEM images of the devices ($x = 0$–30) appear in Figure S6 (Supporting Information).

Twenty-four identical devices were fabricated under the same experimental conditions for the hybrid cation tin perovskites E1Gx with GAI proportions varied from $x = 0$ to $x = 30$; Tables S6–S12 (Supporting Information) list the corresponding PV parameters. **Figure 3**a shows the current–voltage curves and the corresponding IPCE spectra for the best E1Gx cell at each GAI proportion ($x = 0$–30); **Table 1** summarizes the corresponding PV parameters of the best cells and their averaged values. Figure 3b shows box plots of four PV parameters obtained from the 24 identical devices for each E1Gx cell. These results show a slight increasing trend for the mean short-circuit current density (J_{sc}) of the E1Gx devices from $x = 0$ to 10, then slight decreasing for $x > 10$. In contrast, the average open-circuit voltage (V_{oc}) shows similar values for $x = 0$ to 10, but increases progressively with increasing GAI proportions from $x = 15$ to 30. The observed variations of J_{sc} and V_{oc} might

be due to the combined effects of bandgap energies (E_g) and the band alignment, for which the E_g values continuously increase (favoring larger V_{oc}) whereas the energy levels of the VB shift continuously downward upon increasing GAI proportions (Figure 2d) for E1G10 and E1G20 devices for which the energy levels match better with that of the PEDOT:PSS layer (favoring larger J_{sc}). For the FF values, a systematic variation on the FF was observed with the best value occurring at the E1G20 cell. As a result, the device with the best performance is the $GA_{0.2}FA_{0.78}SnI_3$–1% $EDAI_2$ (E1G20) cell that shows average PCE 7.4 ± 0.3% and the best cell PCE 8.5%.

The additive $EDAI_2$ plays an important role in the PV performance of our tin-based hybrid cation planar PSC. We hence used the G20 cell as a reference to fabricate devices with $EDAI_2$ in varied proportions from 0.5% to 2%. Figure S7 (Supporting Information) shows J–V curves of the EγG20 cells with $\gamma = 0$, 0.5, 1, and 2. The poor performance of the G20 cell is obvious, for which PCE was only 0.5% because the perovskite layer has a poor morphology containing many pinholes, according to the top-view SEM shown in Figure S1 (Supporting Information). When the proportion of $EDAI_2$ was increased, the PV performance enhanced substantially, from PCE 3.4% (E0.5G20) increasing to 7.9% (E1G20), and then slightly decreasing to PCE 7.2% (E2G20). This poor performance of the G20 cell is attributed to the poor film coverage that led to serious charge recombination in the device. $EDAI_2$ hence plays an important role to passivate the surface defects, to control the film morphology, and to suppress the oxidation of Sn^{2+} to Sn^{4+}, as reported elsewhere.[26] For our tin-based hybrid cation PSC case, the optimized proportion of $EDAI_2$ is 1%. No hysteresis was observed for both E1 and E1G20 cells according to the J–V scan curves shown in Figure S8 (Supporting Information).

As the stability of a tin-based PSC is a major challenge, we tested the stability of our best cell E1G20 under severe environmental conditions. We first verified the stability of an encapsulated E1G20 device under 1 sun AM1.5G illumination at the
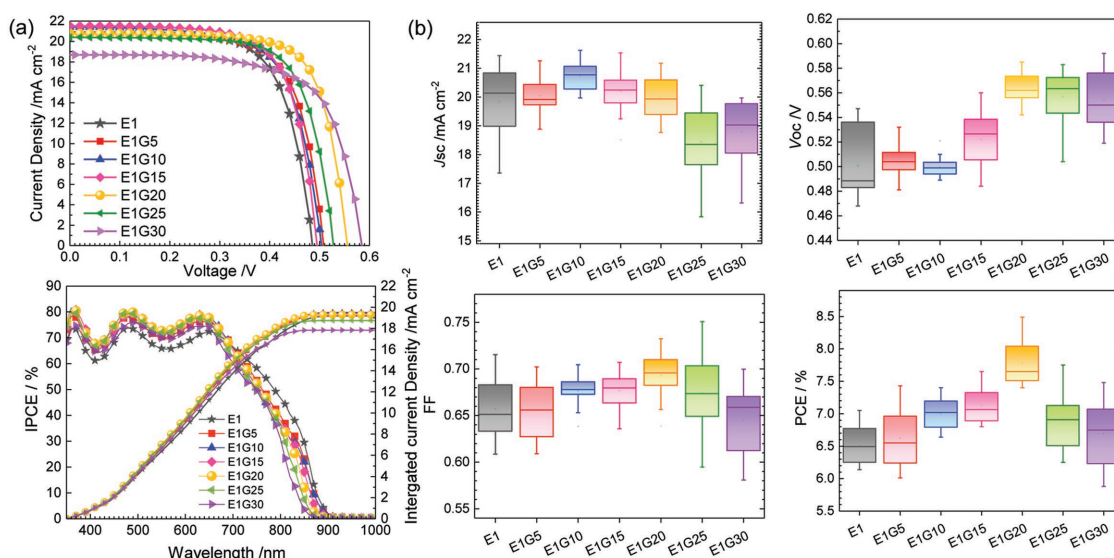

Figure 3. a) Current–voltage curves and corresponding IPCE spectra with integrated current densities, and b) box plots of photovoltaic parameters of 24 cells fabricated under the same experimental conditions for E1Gx ($x = 0$–30) with varied proportions of GAI.

ADVANCED
SCIENCE NEWS
www.advancedsciencenews.com

ADVANCED
MATERIALS
www.advmat.de

Table 1. Photovoltaic parameters of the perovskite solar cells fabricated for the fresh E1Gx cells with the best performance in varied GAI proportions ($x = 0$–30) under simulated AM1.5G illumination (power density 100 mW cm^{-2}). The average values are indicated in parentheses.

Devices	J_{sc} [mA cm^{-2}]	Integration current [mA cm^{-2}]	V_{oc} [V]	FF	PCE [%]
E1	20.9	19.2	0.490	0.693	7.1
	(19.8 ± 1.2)		(0.50 ± 0.02)	(0.657 ± 0.032)	(6.5 ± 0.3)
E1G5	20.8	19.4	0.510	0.697	7.4
	(20.0 ± 0.6)		(0.50 ± 0.01)	(0.656 ± 0.028)	(6.6 ± 0.4)
E1G10	21.4	19.5	0.510	0.684	7.4
	(20.7 ± 0.5)		(0.50 ± 0.01)	(0.676 ± 0.016)	(7.0 ± 0.2)
E1G15	21.5	19.4	0.500	0.694	7.5
	(20.2 ± 0.7)		(0.520 ± 0.02)	(0.677 ± 0.017)	(7.1 ± 0.3)
E1G20	20.8	19.3	0.562	0.726	8.5
	(19.3 ± 0.7)		(0.550 ± 0.01)	(0.696 ± 0.019)	(7.4 ± 0.3)
Best cell[a]	21.2	–	0.619	0.729	9.6
E1G25	20.4	18.7	0.530	0.714	7.8
	(18.4 ± 1.2)		(0.560 ± 0.02)	(0.674 ± 0.04)	(6.9 ± 0.4)
E1G30	18.8	17.8	0.590	0.672	7.5
	(18.7 ± 1.1)		(0.550 ± 0.02)	(0.645 ± 0.034)	(6.7 ± 0.5)

[a]After storage in glove box for 2000 h.

maximum output point in air with humidity RH ≈50%. As the stabilized performance output data shown in **Figure 4**a, the E1G20 device was stable against light illumination for 1 h with negligibly altered PCE and current density; excellent stability of this kind under a rigorous light-soaking condition is remarkable for a pure tin-based PSC. In contrast, for the case of E1 device, the PCE of the device can only sustain for 300 s and then the performance started to deteriorate significantly afterward (inset of Figure 4a). Second, we stored devices E1, E1G20, and pristine FASnI$_3$ in an ambient environment without encapsulation under two conditions, RH 60% and 20%; the results appear in Figure 4b. For RH 60%, the PCE of the pristine FASnI$_3$ device deteriorated to almost naught in 2 h whereas the E1 and E1G20 devices sustained ≈60% and ≈80% of their initial efficiencies after storage for 96 h; both devices deteriorated rapidly after storage for 100 h. In contrast, for the condition RH 20%, the efficiency of the E1 device slightly degraded but the E1G20 device showed almost no degradation after storage period ≈170 h. The superior enduring stability of the unencapsulated E1G20 device in air indicates that the presence of guanidinium as a cocation with zero electric-dipolar moment inside the FASnI$_3$ framework had the effect of retarding the oxidation of perovskite in the presence of moisture. The fabrication of air-stable Sn-based perovskite solar cells has been clearly a challenging task, but we have tackled this problem on incorporating a nonpolar organic cation with an effective additive in a trace proportion. Manipulating the perovskites with moisture-tolerant species is promising strategies toward stable and efficient Sn-based PSC.
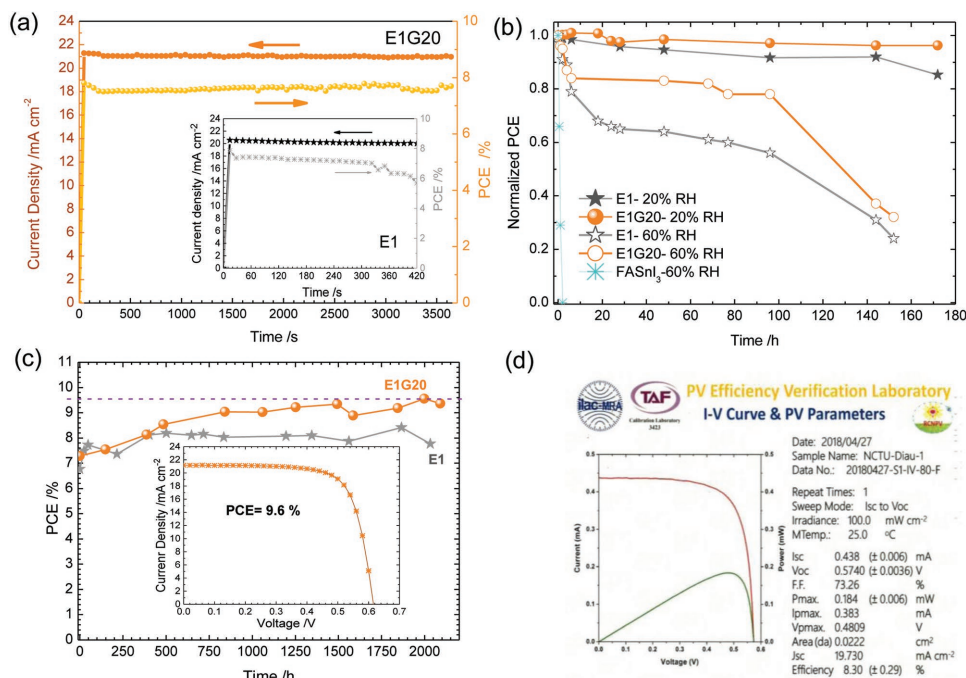

Figure 4. a) Stabilized efficiency of power conversion and photocurrent density of the E1G20 and E1 (shown in the inset) devices taken at the position of maximum power for 1 sun irradiation with AM1.5G solar simulator for 3600 s; enduring stability showing PCE of E1 and E1G20 devices as a function of storage period in two environments: b) ambient air with RH = 20% and 60% without encapsulation, c) N$_2$-filled glove box, and d) certified efficiency 8.30% for the E1G20 device in an ISO-approved PV Efficiency Verification Laboratory in Taiwan.

**ADVANCED
SCIENCE NEWS**

www.advancedsciencenews.com

**ADVANCED
MATERIALS**

www.advmat.de

Both E1 and E1G20 cells were stored inside a glove box to test their device durability as a function of storage period. According to the results shown in Figure 4c, not only they are stable but also their efficiencies increased gradually with increasing storage period. For the E1 device, the PCE increased from 6.8% when freshly prepared up to 8.4% after storage for 2000 h; for the E1G20 device, the PCE increased gradually from initial 7.3% to maximum value 9.6% after storage for 2000 h (Figure S9, Supporting Information). This is the first time that a tin-based perovskite solar cell has attained such a great device performance with outstanding stability. The fresh best cell was sent to a qualified PV Efficiency Verification Laboratory in Taiwan for certification of the device performance under standard testing conditions (STC) following the IEC 60904 procedure to meet the ISO/IEC 17025 standard. The device to be certified was assembled according to a standard procedure shown in Figure S10 (Supporting Information). Even though the verification proceeded under strict conditions, our cell was stable enough to pass all certification steps. A certified performance with PCE = 8.30 ± 0.29% was eventually obtained (Figure 4d; Figure S11, Supporting Information), which marks a new milestone for a tin-based perovskite solar cell to be certified with such great device performance and stability.

Supporting Information

Supporting Information is available online from the Wiley Online Library or from the author.

Conflict of Interest

The authors declare no conflict of interest.

[1] J.-P. Correa-Baena, A. Abate, M. Saliba, W. Tress, T. Jesper Jacobsson, M. Grätzel, A. Hagfeldt, *Energy Environ. Sci.* **2017**, *10*, 710.

[2] W. S. Yang, B.-W. Park, E. H. Jung, N. J. Jeon, Y. C. Kim, D. U. Lee, S. S. Shin, J. Seo, E. K. Kim, J. H. Noh, S. Il Seok, *Science* **2017**, *356*, 1376.

[3] X. Qin, Z. Zhao, Y. Wang, J. Wu, Q. Jiang, J. You, *J. Semicond.* **2017**, *38*, 011002.

[4] L. Liang, P. Gao, *Adv. Sci.* **2018**, *5*, 1700331.

[5] Q. Xu, D. Yang, J. Lv, Y.-Y. Sun, L. Zhang, *Small Methods* **2018**, *2*, 1700316.

[6] Z. Shi, J. Guo, Y. Chen, Q. Li, Y. Pan, H. Zhang, Y. Xia, W. Huang, *Adv. Mater.* **2017**, *29*, 1605005.

[7] K. P. Marshall, M. Walker, R. I. Walton, R. A. Hatton, *Nat. Energy* **2016**, *1*, 16178.

[8] L. M. Herz, *ACS Energy Lett.* **2017**, *2*, 1539.

[9] N. K. Noel, S. D. Stranks, A. Abate, C. Wehrenfennig, S. Guarnera, A.-A. Haghighirad, A. Sadhanala, G. E. Eperon, S. K. Pathak, M. B. Johnston, A. Petrozza, L. M. Herz, H. J. Snaith, *Energy Environ. Sci.* **2014**, *7*, 3061.

[10] F. Hao, C. C. Stoumpos, D. H. Cao, R. P. H. Chang, M. G. Kanatzidis, *Nat. Photonics* **2014**, *8*, 489.

[11] W. Ke, C. C. Stoumpos, I. Spanopoulos, L. Mao, M. Chen, M. R. Wasielewski, M. G. Kanatzidis, *J. Am. Chem. Soc.* **2017**, *139*, 14800.

[12] S. Shao, J. Liu, G. Portale, H.-H. Fang, G. R. Blake, G. H. ten Brink, L. J. A. Koster, M. A. Loi, *Adv. Energy Mater.* **2018**, *8*, 1702019.

[13] Y. Liao, H. Liu, W. Zhou, D. Yang, Y. Shang, Z. Shi, B. Li, X. Jiang, L. Zhang, L. N. Quan, R. Quintero-Bermudez, B. R. Sutherland, Q. Mi, E. H. Sargent, Z. Ning, *J. Am. Chem. Soc.* **2017**, *139*, 6693.

[14] S. J. Lee, S. S. Shin, Y. C. Kim, D. Kim, T. K. Ahn, J. H. Noh, J. Seo, S. Il Seok, *J. Am. Chem. Soc.* **2016**, *138*, 3974.

[15] K. Chen, P. Wu, W. Yang, R. Su, D. Luo, X. Yang, Y. Tu, R. Zhu, Q. Gong, *Nano Energy* **2018**, *49*, 411.

[16] W. Ke, C. C. Stoumpos, M. Zhu, L. Mao, I. Spanopoulos, J. Liu, O. Y. Kontsevoi, M. Chen, D. Sarma, Y. Zhang, M. R. Wasielewski, M. G. Kanatzidis, *Sci. Adv.* **2017**, *3*, e1701293.

[17] C.-M. Tsai, N. Mohanta, C.-Y. Wang, Y.-P. Lin, Y.-W. Yang, C.-L. Wang, C.-H. Hung, E. W.-G. Diau, *Angew. Chem., Int. Ed.* **2017**, *56*, 13819.

[18] F. Wang, J. Ma, F. Xie, L. Li, J. Chen, J. Fan, N. Zhao, *Adv. Funct. Mater.* **2016**, *26*, 3417.

[19] T. Shi, H.-S. Zhang, W. Meng, Q. Teng, M. Liu, X. Yang, Y. Yan, H.-L. Yip, Y.-J. Zhao, *J. Mater. Chem. A* **2017**, *5*, 15124.

[20] Z. Zhao, F. Gu, Y. Li, W. Sun, S. Ye, H. Rao, Z. Liu, Z. Bian, C. Huang, *Adv. Sci.* **2017**, *4*, 1700204.

[21] D. H. Cao, C. C. Stoumpos, T. Yokoyama, J. L. Logsdon, T.-B. Song, O. K. Farha, M. R. Wasielewski, J. T. Hupp, M. G. Kanatzidis, *ACS Energy Lett.* **2017**, *2*, 982.

[22] G. Kieslich, S. Sun, A. K. Cheetham, *Chem. Sci.* **2015**, *6*, 3430.

[23] D. Yang, J. Lv, X. Zhao, Q. Xu, Y. Fu, Y. Zhan, A. Zunger, L. Zhang, *Chem. Mater.* **2017**, *29*, 524.

[24] G. Giorgi, J.-I. Fujisawa, H. Segawa, K. Yamashita, *J. Phys. Chem. C* **2015**, *119*, 4694.

[25] C. C. Stoumpos, L. Mao, C. D. Malliakas, M. G. Kanatzidis, *Inorg. Chem.* **2017**, *56*, 56.

[26] E. Jokar, C.-H. Chien, A. Fathi, M. Rameez, Y.-H. Chang, E. W.-G. Diau, *Energy Environ. Sci.* **2018**, *11*, 2353.

[27] T. Li, Y. Pan, Z. Wang, Y. Xia, Y. Chen, W. Huang, *J. Mater. Chem. A* **2017**, *5*, 12602.

[28] T. Sato, S. Takagi, S. Deledda, B. C. Hauback, S. Orimo, *Sci. Rep.* **2016**, *6*, 23592.

[29] D. J. Kubicki, D. Prochowicz, A. Hofstetter, M. Saski, P. Yadav, D. Bi, N. Pellet, J. Lewiński, S. M. Zakeeruddin, M. Grätzel, L. Emsley, *J. Am. Chem. Soc.* **2018**, *140*, 3345.

[30] C. Yi, J. Luo, S. Meloni, A. Boziki, N. Ashari-Astani, C. Grätzel, S. M. Zakeeruddin, U. Röthlisberger, M. Grätzel, *Energy Environ. Sci.* **2016**, *9*, 656.

[31] W.-G. Li, H.-S. Rao, B.-X. Chen, X.-D. Wang, D.-B. Kuang, *J. Mater. Chem. A* **2017**, *5*, 19431.

[32] E. C. Schueller, G. Laurita, D. H. Fabini, C. C. Stoumpos, M. G. Kanatzidis, R. Seshadri, *Inorg. Chem.* **2018**, *57*, 695.

[33] T. M. Koh, T. Krishnamoorthy, N. Yantara, C. Shi, W. L. Leong, P. P. Boix, A. C. Grimsdale, S. G. Mhaisalkar, N. Mathews, *J. Mater. Chem. A* **2015**, *3*, 14996.

[34] Y. Dang, Y. Zhou, X. Liu, D. Ju, S. Xia, H. Xia, X. Tao, *Angew. Chem., Int. Ed.* **2016**, *55*, 3447.

[35] A. D. Jodlowski, C. Roldán-Carmona, G. Grancini, M. Salado, M. Ralaiarisoa, S. Ahmad, N. Koch, L. Camacho, G. De Miguel, M. K. Nazeeruddin, *Nat. Energy* **2017**, *2*, 972.

[36] S. Bae, S. J. Han, T. J. Shin, W. H. Jo, *J. Mater. Chem. A* **2015**, *3*, 23964.

[37] F. Hao, C. C. Stoumpos, P. Guo, N. Zhou, T. J. Marks, R. P. H. Chang, M. G. Kanatzidis, *J. Am. Chem. Soc.* **2015**, *137*, 11445.

[38] W. Liao, D. Zhao, Y. Yu, C. R. Grice, C. Wang, A. J. Cimaroli, P. Schulz, W. Meng, K. Zhu, R.-G. Xiong, Y. Yan, *Adv. Mater.* **2016**, *28*, 9333.